Influence of plastic anisotropy and strain path on strain-induced phase transformation of cobalt

Pierre-Antoine Dubos, Jamal Fajoui, Baptiste Girault, David Gloaguen

Influence of plastic anisotropy and strain path on strain-induced phase transformation of cobalt

Pierre-Antoine DUBOS[a*], Jamal FAJOUI[a], Baptiste GIRAULT[a], David GLOAGUEN[a]

[a] Nantes Université, Ecole Centrale Nantes, CNRS, GeM, UMR 6183, F-44600 Saint-Nazaire, France.

*Corresponding author: pierre-antoine.dubos@univ-nantes.fr

On behalf of all authors, the corresponding author states that there is no conflict of interest.

Graphical abstract: Evolution of metastable cobalt FCC volume proportion during mechanical loading.

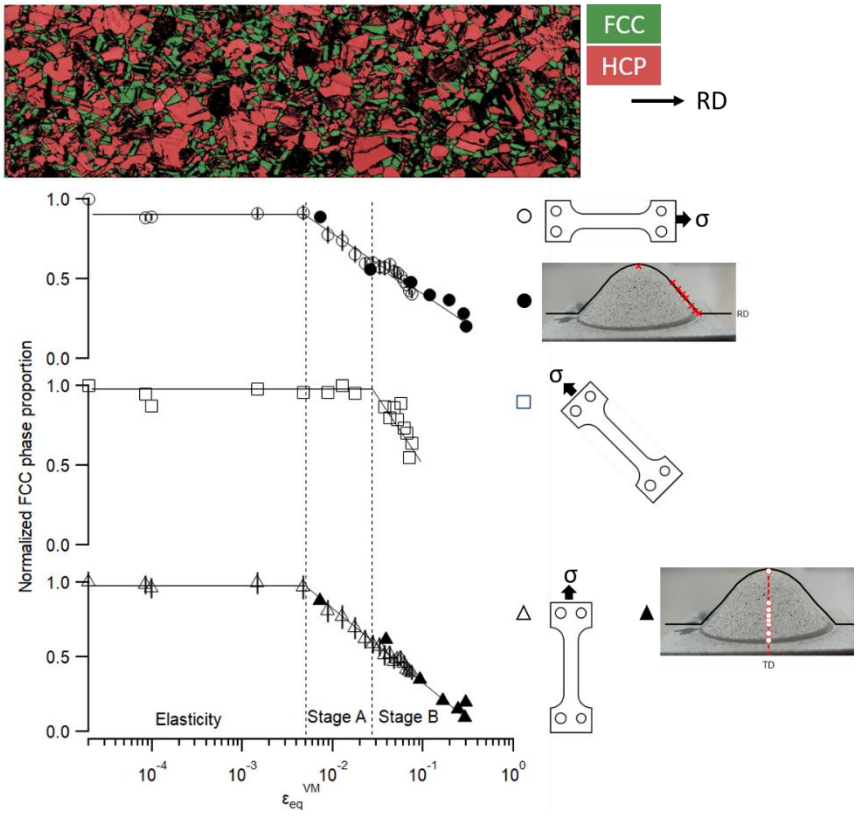

Abstract

The objective of this paper is to contribute to a better understanding of the deformation mechanisms of a rolled polycrystalline cobalt sheet. In order to achieve this goal, a particular

attention is given to the strain-induced phase transformation and the forming parameters on which it may depend such as the plastic anisotropy or the loading path.

In situ phase quantification by X-ray diffraction during tensile tests, on samples cut out from a cold rolled sheet material in three different directions (at 0°, 45° and 90° from the rolling direction), has enabled to study the influence of plastic anisotropy on the strain-induced phase transformation of metastable retained Face Centered Cubic phase to Hexagonal Close Packed phase. Results show that the martensitic phase transformation can be activated by basal slip in the first stage of plasticity but it also indicates that the latter is delayed when sample is strained in tension for an angle of 45° to the rolling direction. *Post mortem* analyses on a stamped sample by the Nakazima test have revealed that the phase transformation continues for higher strain levels. A particular interest is paid to the coupling between strain-hardening mechanisms and phase transformation and is discussed given the plastic anisotropy of cobalt aggregate.

Keywords: cobalt, mechanical properties, anisotropy, phase transformation, X-ray diffraction

1. Introduction

Work-hardening mechanisms of Hexagonal Closed-Packed (HCP) cobalt are quite specific due to the *c/a* ratio close to the ideal value, the high melting temperature [1] and the low stacking fault energy [2]. Basal dislocation glide on the $\{00.1\}\langle 1\bar{2}.0\rangle$ crystallographic system is the first stage of cobalt work hardening and it has been extensively studied in the 50s and 60s by Seeger *et al.*[3–5]. Due to the limited number of available slip systems, the plastic deformation is quickly accommodated by the twinning process as the second stage of

work hardening. More recently, in the 2010s, Martinez *et al.* [6–9] and Zhu *et al.* [10,11] have studied more specifically the key-role of twinning to accommodate plastic deformation.

HCP cobalt presents an allotropic transformation to Face Centered-Cubic (FCC) for temperatures higher than 440 °C while the reverse martensitic transformation temperature is around 330 °C, exhibiting a hysteresis. This transformation is not fully reversible and the metastable FCC phase remains generally present at room temperature. This allotropic transformation, caused by temperature, has been extensively studied in the 1970s and from the 1990s to 2010 [12–31]. The retained FCC phase is mechanically unstable under stress unless it has undergone a specific heat treatment under controlled time and temperature conditions (long time combined with high temperatures) [8,32]. The properties of cobalt, both mechanical and magnetic, have also been extensively studied [1,32–39]. Some original effects such as sensitivity to size effects [8,39,40] or non-linear elasticity [38,41] have been the subject of recent studies. However, only few studies have focused on two-phase effect with the exception of one which showed that the presence of the residual FCC phase was beneficial to the mechanical properties [33]. This brief study does not mention the mechanical stability of the microstructure with heat treatments and was therefore not interested in the possible phase transformation induced by the mechanical deformation.

The strain-induced FCC to HCP phase transformation in cobalt has rarely been investigated since Sanderson's work in the 1970s [32]. Only a few recent works on thin films [42] and on the influence of temperature [43], deal nevertheless with this mechanism [32,42,43]. Concerning the cobalt alloys, the study on a Co-Ni-Cr-Mo alloy shows a correlation between deformation modes, stacking fault energy and strain-induced phase transformation [44]. On Co-Cu alloys, a full FCC to HCP transformation has been observed for a severe plastic deformation process [45]. These investigations agree that the residual FCC phase can be

transformed into HCP phase by plastic deformation at room temperature, provided that it has not been stabilized by a heat treatment.

Dubos *et al.* [46,47] have investigated the size effects in complex forming processes of different high-purity metals. For mechanically stabilized microstructure of polycrystalline cobalt, first results exhibit a strain path dependence of size effects during stamping tests. This deformation process can actually be used for the microforming of miniaturized systems in which cobalt can be a good candidate due to its specific mechanical and magnetic properties. The fields of application can be varied such as sensors, electronics, micro-mechanics, medical, *etc*.

These previous works clearly show a renewed interest in this material, despite the complexity of its deformation mechanisms and the little-studied phenomena such as plasticity-induced phase transformation when the microstructure is not mastered beforehand.

Plastic anisotropy is an extremely important factor to be considered in sheet metal forming. The most studied HCP phase metals (i.e. magnesium, zirconium and titanium) display strong plastic anisotropy which results in a Lankford coefficient varying between 2 and 4 [48]. This plastic anisotropy directly results from the marked rolling texture of HCP metal sheets [49]. For polycrystalline cobalt, Lankford coefficient is around 0.92 (weak plastic anisotropy). Nevertheless, it is strongly influenced by the microstructure, notably the grain size [47].

The main aim of this experimental study is to contribute to the knowledge and the understanding of the strain-induced phase transformation in cobalt when the FCC retained phase is mechanically unstable. After a detailed description of the experimental methods, focusing on X-Ray Diffraction (XRD) phase quantification and mechanical tests carried out

(tensile and stamping tests), results are given to highlight the influence of plastic anisotropy and the strain path deviation on the FCC to HCP phase transformation induced by plasticity. *Post mortem* phase quantifications will be presented on a stamped sample which displays a high strain gradient and will be compared to those obtained by tensile tests in different directions by considering von Mises equivalent strain. Finally, the plastic anisotropy effect will be discussed in view of activation and transformation rate. In a second step, the influence of plastic anisotropy on the main work-hardening mechanisms and on the competition between twinning and phase transformation will be raised.

2. Material and methods

Commercial polycrystalline cobalt sheets (Goodfellow Company) of high-purity (99.9 wt. %), cold-rolled to 0.5 mm in thickness in a recrystallized state, were used for the present study. Electron Back Scattered Diffraction (EBSD) mapping has been performed (**Fig. 1 (a)**) in order to obtain initial grain size and phase cartographies. The initial ratio between the two phases is around 70 % HCP / 30 % FCC with corresponding grains sizes of 30 ± 20 µm and 14 ± 10 µm.

The calculation of the grain size is performed on each phase, only with the indexed pixels. There seems to be no correspondence between the band contrast and the non-indexed pixels. This confirms the recrystallized state of the sheet after cold rolling and the absence of significant residual stresses.

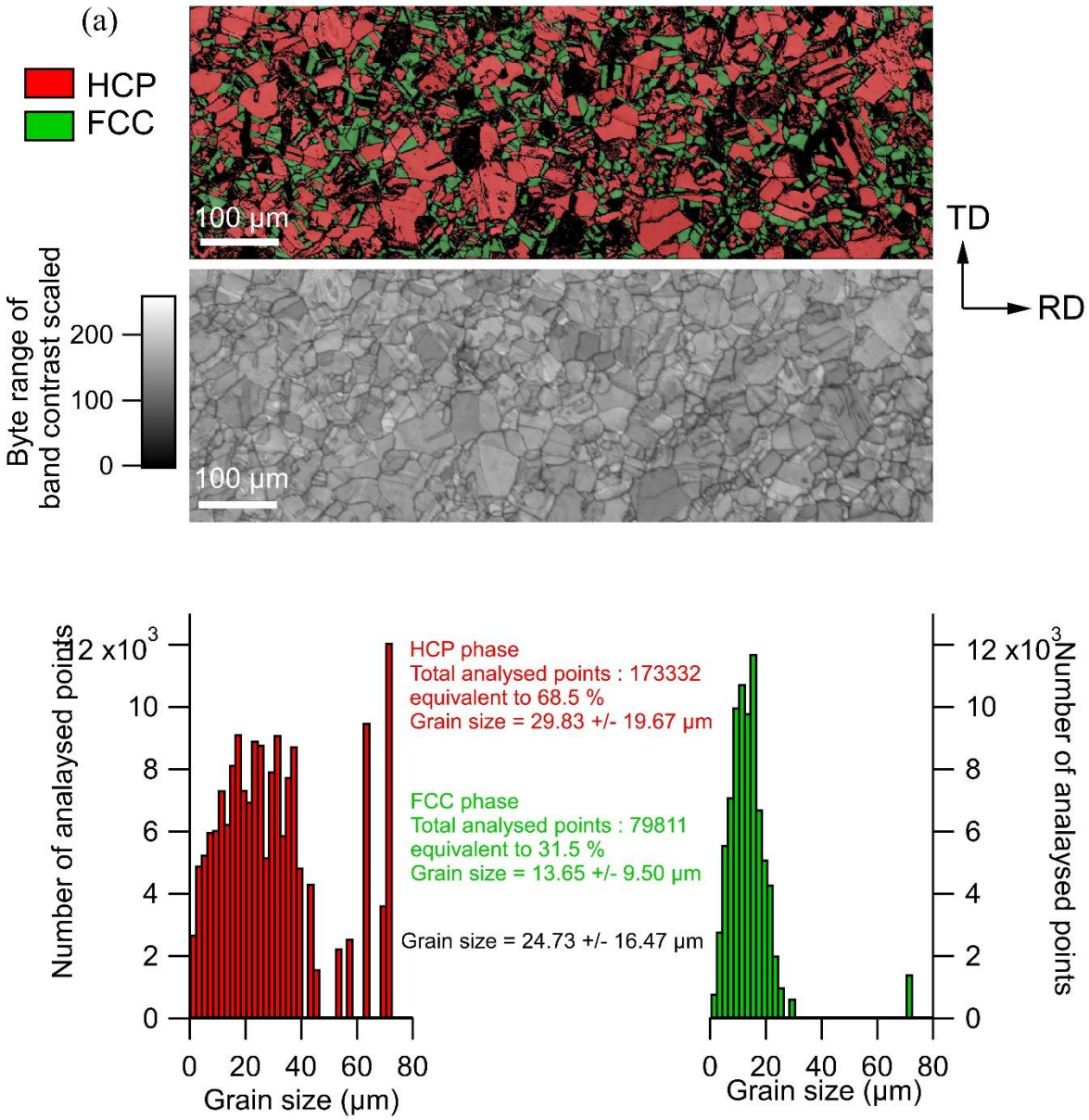
(a)
HCP
FCC
100 µm
TD
RD
Byte range of band contrast scaled
200
100
0
100 µm
Number of analysed points
12 x10^3
10
8
6
4
2
0
0 20 40 60 80
Grain size (µm)
HCP phase
Total analysed points : 173332
equivalent to 68.5 %
Grain size = 29.83 +/- 19.67 µm
FCC phase
Total analysed points : 79811
equivalent to 31.5 %
Grain size = 13.65 +/- 9.50 µm
Grain size = 24.73 +/- 16.47 µm
12 x10^3
Number of analysed points
0 20 40 60 80
Grain size (µm)

109

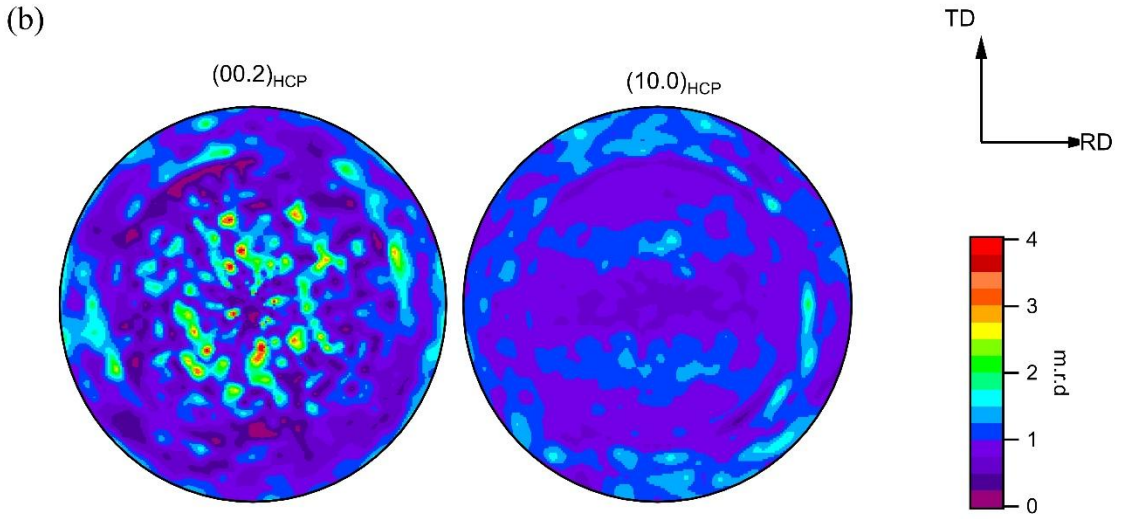

Figure 1: Microstructural analysis of the as-received material**:** (a) EBSD map of phase distribution and band contrast. Distribution of grain size for each phase. HCP phase is colored in red and FCC phase in green. (b) XRD crystallographic textures of the HCP phase determined from the orientation distribution functions calculated by the WIMW method implanted in the BEARTEX software.

Crystallographic textures and retained FCC phase ratios, at room temperature, were determined by XRD technique. A four-circle Seifert XRD3003 PTS diffractometer equipped with a Euler cradle, a Position Sensitive Detector (PSD) with a 2θ effective windows of 8.6°, a 1 mm diameter collimator and an IDS camera (for sample positioning in the center of the goniometer), was used. A Cr anode ($CrK_{\alpha 1+2}$ radiation), operating at 30 kV and 35 mA, was used (wavelength λ = 2.28964 Å). The K_β component of the Cr radiation was eliminated using a vanadium filter installed in front of the detector.

Experimental XRD peak profiles were fitted by a Pseudo-Voigt function which takes into account the $K_{\alpha 1}$-$K_{\alpha 2}$ doublet [50]. For each diffraction peak, background was modeled through a 2nd order polynomial function. Prior to peak profile analysis, angular corrections (Lorentz, polarization and absorption factors) have also been applied [51].

Fig. 1 (b) shows recalculated $\{00.2\}_{HCP}$ and $\{10.0\}_{HCP}$ Pole Figures (PFs) of the as-received sample. The crystallographic textures have been determined from the Orientation Distribution Functions (ODF) calculated by the WIMV method implemented in the BEARTEX software [52], and were obtained from $\{10.0\}_{HCP}$, $\{00.2\}_{HCP}$, $\{10.1\}_{HCP}$ and$\{10.2\}_{HCP}$ experimental PFs with an average error coefficient of about 0.08. This initial state displays a slight centered basal reinforcement of ($\{00.2\}_{HCP}$ on Fig. 1 (b)) with symmetrical intensity distribution of ($\{00.2\}_{HCP}$ and $\{10.0\}_{HCP}$ on Fig. 1 (b)) representative of a rolling texture for hexagonal materials with a *c/a* ratio close to 1.633. The central pole of $\{00.2\}_{HCP}$ in Fig. 1 (b) is distributed up to an angle of 43.1° characteristic of the habit plane between the two phases considering the Shoji-Nishiyama's relation [10].

The FCC phase volume fraction (denoted f^{FCC}) has been determined for each measurement point using the equation (1) as formulated by Shang *et al.* [53]:

$$f^{FCC} = \left(1 + \frac{I_{hkl}^{HCP}}{I_{hkl}^{FCC}} \frac{R_{hkl}^{FCC}}{R_{hkl}^{HCP}}\right)^{-1} \quad (1)$$

where I_{hkl} is the integrated intensity of the corresponding $\{hkl\}$ peak. R_{hkl} is the reflectivity of the lattice plane $\{hkl\}$, and is given by the following equation (2) introduced in the literature [54]:

$$R_{hkl} = \frac{1}{v^2} |F_{hkl}|^2 \left(\frac{1 + \cos^2(2\theta)}{\sin^2(2\theta)\cos(\theta)}\right) m \frac{e^{-2M}}{\mu} \quad (2)$$

where v is the volume of the crystal unit cell (in $Å^3$), F_{hkl} is the structure factor, 2θ is the considered Bragg angle (in rad), m is the $\{hkl\}$ planes multiplicity factor, μ is the linear absorption coefficient (in cm^{-1}) and e^{-2M} is the Debye-Waller factor [1,55].

147 The volume fraction of the phases was calculated from several groups of family planes,
148 combining $\{10.0\}_{HCP}$, $\{00.2\}_{HCP}$, $\{10.1\}_{HCP}$, $\{10.2\}_{HCP}$ and $\{111\}_{FCC}$, $\{200\}_{FCC}$, and
149 averaged.

150 *In situ* monotonic uniaxial tensile tests were carried out, at room temperature, to study the
151 influence of elastoplastic strain on the allotropic transformation. These mechanical tests were
152 performed on a DEBEN device with a load cell of 5 kN capacity and controlled by the
153 displacement between clamping jaws. The dog bone shaped tensile specimens were machined
154 by electrical discharge machining and designed a gauge section of 26 mm in length, 7 mm in
155 width and 0.5 mm in thickness in three different directions having an angle α with respect to
156 the Rolling Direction (RD) of the sheet: 0°/RD, 45°/RD and 90°/RD, latter corresponding thus
157 to the Transverse Direction (TD).

158 In order to quantify the evolution of the phase ratio during the tensile loading, the samples
159 were strained stepwise up to 7.8 % with a strain rate of 0.2 mm/min (quasi-static deformation
160 hypothesis). At each straining step, and after a stress relaxation of about 20 minutes ensuring
161 stable mechanical fields over the entire diffracting volume, X-ray diffraction analyses were
162 carried out at each measurement point.

163 To obtain the macroscopic mechanical response, a second mechanical test series was achieved
164 where the specimens were continuously strained up to 7.8 % with a strain rate of 0.2 mm/min.
165 On one side of the sample, longitudinal and transverse deformations were measured with
166 strain gauges in order to obtain the Young modulus *E* and the Poisson's coefficient *v*. On the
167 other side of the specimen, a speckle was deposited and images were recorded during the test.
168 Digital Image Correlation (DIC) has then been processed to obtain the macroscopic total
169 strain fields during the mechanical tests. Images were recorded with a Point-Grey GS3-U3
170 camera with 2448×2048 px² resolution and a lens of 35 mm. DIC has been performed with

VIC 2D software using a region of interest of 155×37 px² (i.e. 26.35×6.29 mm² with a pixel size of 0.17 mm), a subset of 9×7 px² and a grid step of 1×1 px². Planar strain fields were computed in order to obtain the ε_{xx} and ε_{yy} strain components along the tensile and the transverse directions, respectively. For each sample, the plastic anisotropy coefficient (also called Lankford) was calculated from the monotonic plastic regime with the following Eq. (3), considering a plastic incompressibility [56,57]:

$$r_\alpha = \frac{\varepsilon_{yy}^p}{\varepsilon_{zz}^p} = -\frac{\varepsilon_{yy}^p}{\varepsilon_{xx}^p + \varepsilon_{yy}^p} \quad (3)$$

α being the angle between the RD and the specimen axes.

With these measurements, corresponding strain paths can be characterized with the parameter β which can be expressed by:

$$\beta_\alpha = \frac{\varepsilon_{yy}}{\varepsilon_{xx}} \quad (4)$$

Combining equations (3) and (4) the strain path can be directly introduced as a function of the Lankford coefficient in the following relationship:

$$\beta_\alpha = -\frac{r_\alpha}{1+r_\alpha} \quad (5)$$

The mean Lankford coefficient r_{mean}, relative to the mean anisotropy of the sheet, and Δr, representative of the planar anisotropy, are respectively calculated thanks to equations (6) and (7):

$$r_{mean} = \frac{r_{0°} + 2r_{45°} + r_{90°}}{4} \quad (6)$$

$$\Delta r = \frac{r_{0°} - 2r_{45°} + r_{90°}}{2} \quad (7)$$

Table 1 gives these coefficients for the three analyzed directions. In accordance with previous results [47], the as-received cobalt displays a mean Lankford coefficient of 0.9 indicating a mild plastic anisotropy. In this table, $|\beta-\beta_{iso}|$ represents the relative deviation of the strain path as compared to the isotropic case (β_{iso} **= -0.5)**. The analysis of these parameters reveals a qualitative difference of the material behavior when the sample is strained at 45°/RD.

Table 1: Review of the main coefficients characterizing elastic and plastic anisotropies determined for polycrystalline specimens (E: Young modulus, v: Poisson coefficient, α: direction of specimen collection, r: Lankford coefficient, β; strain path, $|\beta-\beta_{iso}|$: strain path deviation, r_{mean}: mean plastic anisotropy coefficient, Δr: planar plastic anisotropy coefficient).

	0°/RD (RD)	**45°/RD**	**90°/RD (TD)**
***E* [GPa]**	167	181.3	152
***u(E)* [GPa]**	14	3.8	19
v	0.32632	0.38573	0.38712
u(v)	0.00023	0.00069	0.00078
r_α	0.8110	0.77344	1.242
$u(r_\alpha)$	0.0034	0.00057	0.022
β	-0.4491	-0.43617	-0.5579
$u(\beta)$	0.0011	0.00018	0.0090
$\lvert\beta-\beta_{iso}\rvert$	0.0509	0.06383	0.0579
r_{mean}		0.9000	
Δr		0.2531	

Stamping test, also named Nakazima test, is a complex biaxial loading experiment that enables to obtain various loading conditions in only one test. Nakazima tests were performed with a universal sheet metal testing machine (Zwick Roell BUP 600) on the as-received cobalt

sheet using a 20 mm hemispherical punch at a punch speed of 1 mm/s. The ratio of punch radius on sheet thickness is large enough to assume plane-stress deformations. Blank holder force was set to 3000 N to ensure no sliding. To reduce friction effect between the punch and the sample, a grease/polytetrafluoroethylene/grease sandwich was employed. Strain fields were measured during the tests using 3D DIC. The experimental procedures for these tests are described with more details in previous works [46,47]. XRD analyses have been performed on stamped samples along RD and TD in order to follow the retained FCC phase evolution under a complex loading. For each measurement point, the irradiated area has been reduced (a circle with a diameter of 1 mm) with a Pb masking to avoid the geometric errors associated to the curved surface. **Fig. 2** shows the location of the XRD analysis points on the stamped dome (a). The three principal components of the strain fields are presented along a section of the stamped dome (b). ε_{III} is calculated with the plastic imcompressibilty assumption ($\varepsilon_{III} = -\varepsilon_{I}-\varepsilon_{II}$). The weak plastic anisotropy, combined with residual friction, induces a slight deviation of the strain path. A strain path gradient along the section of the stamped dome is revealed and must be considered (c). The equibiaxiality of the loading is increased between the blank holder and the top of the punch. This test allows to obtain a macroscopic equivalent strain gradient along a section that could induce a composition gradient in terms of phase proportion. The equivalent strain level is higher, (around *0.3*), than the maximum strain that could be reached with a tensile test.

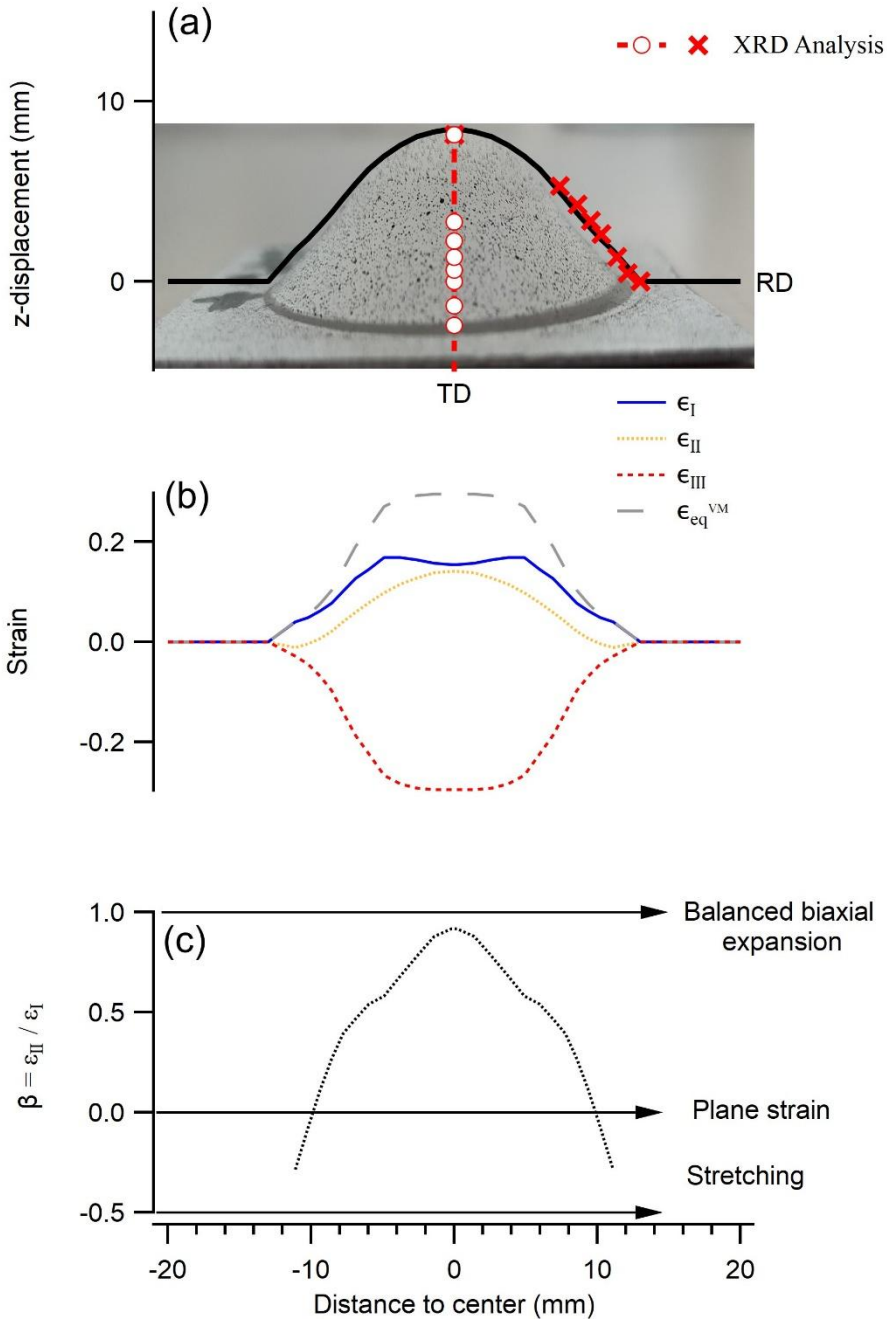

Figure 2: Description of the Nakazima test: (a) height of the part after stamping and location of the analysis points by XRD (cross and circle marker for measurements in RD and TD, respectively), (b) decomposition of the principal components of the macroscopic strain fields (ε_I: in-plane major strain (along RD), ε_{II}: in-plane minor strain (along TD), ε_{III}=-ε_I- ε_{II}: in the thickness strain and corresponding ε_{eq} von Mises equivalent strain), (c) evolution of the strain path β versus the location on the section.

3. Results and discussion

3.1. Influence of the plastic anisotropy

Retained FCC phase proportion and work-hardening rate ($\theta = d\sigma/d\varepsilon$) evolutions with the macroscopic strain, ε, applied during tensile tests for the three considered directions (0°/RD, 45°/RD and 90°/RD) are plotted in **Fig. 3**. The calculated value of r_α is indicated on this figure.

Work-hardening curves exhibit two distinct stages after elasticity. Basal dislocation slip is the dominant mechanism in the stage A [8] while twinning mechanisms occur in stage B to accommodate plastic deformation [7]. Results from **Fig. 3** show that anisotropy does not seem to affect the work-hardening stages. No matter the misorientation set between the loading axis and the RD, elastic strain does not allow for the phase transformation to be initiated. For α = 0° and 90°, FCC to HCP phase transformation is initiated in stage A of plasticity. Beyond that, the initial retained FCC phase transforms into HCP phase in a linear way to the logarithm of the strain. At a macroscopic strain of 7.8 %, approximately 60 % of the initial retained FCC phase is strain-induced transformed. For $\alpha = 45°$, the initiation of the phase transformation is delayed to the stage B. For this particular direction, twinning mechanisms seem to initiate the FCC to HCP phase transformation. The plastic deformation transforms about 40 % of the initially present FCC phase at 7.8 %.

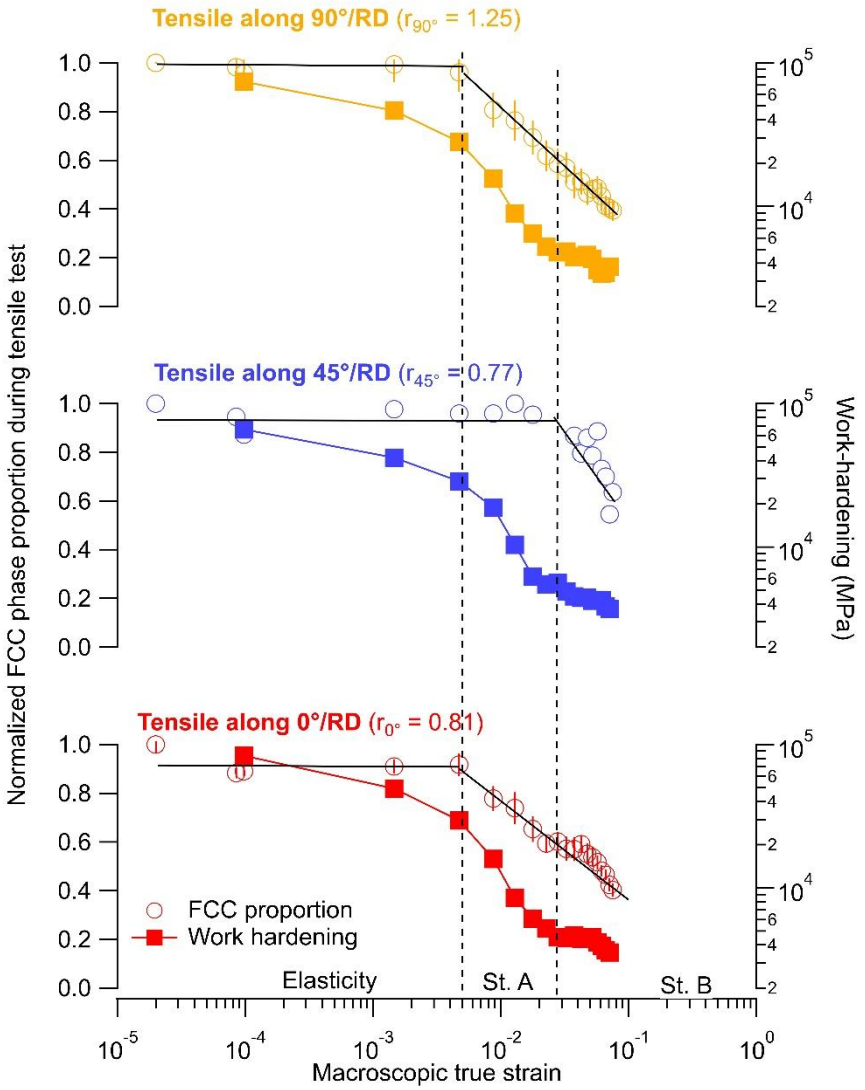

Figure 3: FCC phase proportion (normalized to the initial retained FCC phase) and work-hardening rate evolutions under tensile testing for different angles between the load axis and the rolling direction (RD): 0° /RD (RD), 45° /RD and 90° /RD (TD°).

The evolution of the FCC phase ratio with the macroscopic strain can be summarized by the following equation:

$$\frac{\%FCC}{\%FCC_{init}} = \begin{cases} cst \approx 1 \; if \; \varepsilon < \varepsilon_{init}(\alpha) \\ A(\alpha) + m(\alpha) \times \log(\varepsilon) \; if \; \varepsilon > \varepsilon_{init}(\alpha) \end{cases} \quad (8)$$

where $A(\alpha)$ is a constant which depends on the orientation of the sample regarding the RD and $m(\alpha)$ is the slope of the normalized phase ratio which can be assimilated to a rate of

transformation with the strain. $\varepsilon_{init}(\alpha)$ matches the strain at which the phase transformation initiates. These values are presented in **Table 2** for each direction.

Table 2: Coefficients of equation (8) with standard deviations (u) and linear regression coefficient (R^2) as a function of the loading axis misorientation regarding the RD.

	α = 0°/RD° (RD)	α = 45°/RD	α = 90°/RD° (TD)
m	-0.373	-0.80	-0.459
u(m)	0.022	0.11	0.012
A	0.027	-0.25	-0.120
u(A)	0.033	0.14	0.019
R²	0.95	0.93	0.99
ε_{init}	0.00247	0.0281	0.00365

In a recent work [43], it has been shown that, for a particular direction (in this case, RD), ε_{init} increases with temperature. However, the transformation rate is independent for temperatures lower than the initiation temperature of austenitic transformation. Sanderson [32] has shown that m(α) is strongly affected by the initial microstructure (grain size and initial FCC proportion). Marx *et al.* [42] have highlighted that the integrated area of the $\{002\}_{FCC}$ reflection decreases with macroscopic strain until a plateau is forming for strains higher than 8 %. These observations tend to highlight a threshold deformation at which the residual FCC phase no longer transforms. Unfortunately, the critical macroscopic strain reached in our work for tensile tests does not allow us to confirm this phenomenon. In order to track the phase transformation for macroscopic equivalent strain higher than 7.8 %, a stamping test, whose methodology was described in the previous section, was performed.

3.2. Influence of the mechanical loading on the allotropic transformation

As shown in **Fig. 2**, *post-mortem* XRD analyses have been performed at different locations on the stamped dome between the blank-holder and the top of the punch. Strain path, and therefore equivalent strain level, is dependent on the chosen measurement point. In order to consider the plastic anisotropy effect, phase quantification has been achieved along two directions (RD and TD).

Fig. 4 displays the evolution of the FCC phase ratio normalized by the initial retained FCC phase versus the equivalent macroscopic von Mises strain for the two directions RD and TD on the stamped sample (filled points). These results are superimposed on those obtained in tension for specimens taken with an angle $\alpha = 0°$ and 90° (empty points).

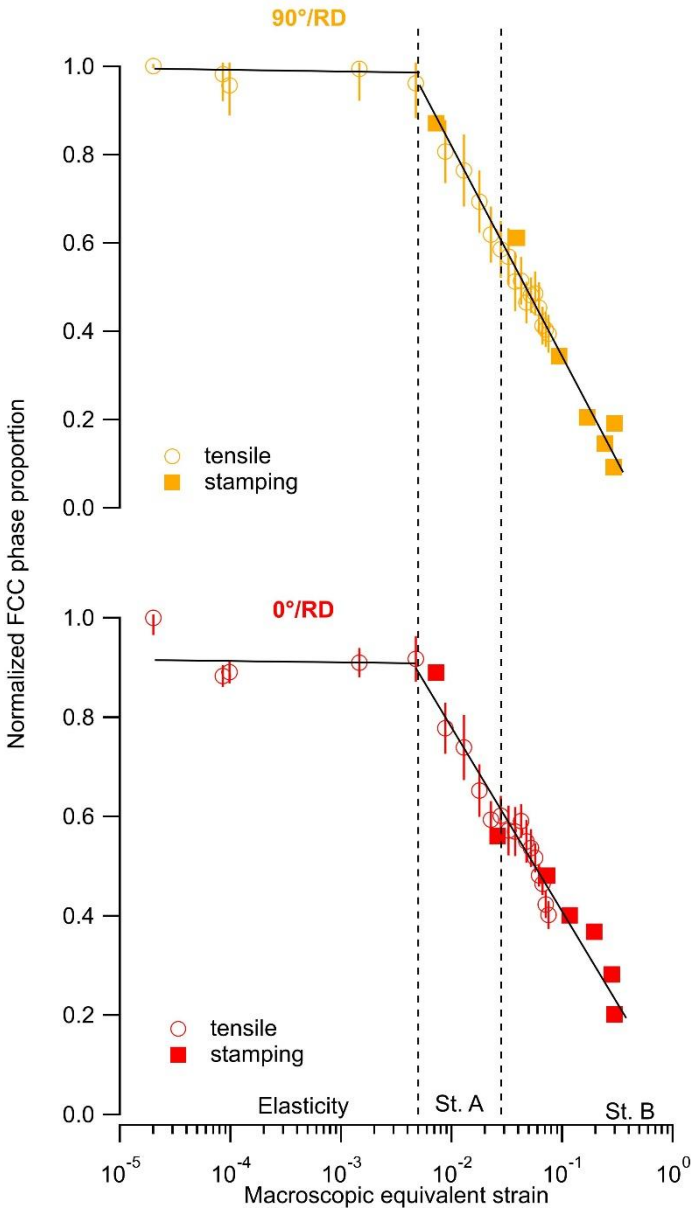

Figure 4: Influence of different biaxial loading scenarios on the phase transformation. Evolution of the FCC phase ratio along the rolling and transverse directions (filled squares) of a stamped sample, superposed on the *in situ* tensile test results (circles).

The transformation rate is shown to be independent from the strain path but slightly direction-dependent. During stages A and B of plasticity, the FCC phase proportion decreases linearly with the logarithm of the von Mises' equivalent strain. The slopes are the same as those obtained with tensile tests and therefore always dependent on α angle. The maximum strain reaches about 30 % in the center of the Nakazima specimen, resulting in a transformation of

around 70 % of the FCC phase initially retained. Straumal *et al.* showed that a complete transformation was possible in Co-Cu alloys deformed by severe plastic deformation processes such as high-pressure torsion (HPT). These authors estimated that a severe plastic shear strain higher than 35 % could achieve a full FCC to HCP phase transformation [45]. Extrapolating the evolution law obtained from our results with the stamping tests, a complete transformation of the initially present FCC phase can only be expected for very high levels of plastic strain, in the order of 100 %. Finally, the main point is that the strain-induced FCC to HCP phase transformation continues for higher strain level than the one reached by previous tensile tests.

3.3. Relation between plastic anisotropy, strain path and phase transformation rate.

Fig. 5 displays the slope of the strain-induced transformation, $m(\alpha)$, for tensile tests, plotted for the three considered values of α, versus the absolute value of β-β_{iso}. Latter is representative of the strain path deviation due to anisotropy as compared to the strain path of the isotopic case. The deviation of r_α from 1 significantly affects the strain path: for a tensile loading, if r_α is higher than 1, the loading conditions is close to plane strain ones, while if r_α is lower than 1, the loading conditions tend to shear ones. The strain path seems to be less affected in the case of a positive r_α variation (values above the isotropic case i.e. r_α = 1) than a negative one (r_α values below 1). For a value of r_α = 1.25, the positive variation of 0.25 results in a 11 %deviation of the strain path. For a value of r_α = 0.75, the deviation is negative and equal to -0.25 and results in a 14 %deviation of the strain path. These two examples are respectively representative of the cases with α = 90° and α = 45°.

$m(\alpha)$ exhibits a linear decrease with increasing strain path deviation. **Fig. 5** illustrates the strong impact of $|\beta-\beta_{iso}|$ value on $m(\alpha)$. For α = 45°, which presents a slightly lower negative value of r_α variation than for α = 0° and a sign variation from the isotropic case opposite to $r_{90°}$, the transformation rate is almost twice higher. This tends to be in line with the results obtained by Straumal *et al.* [45]. Indeed, for shear loading conditions, the deformation level required to transform the same volume of FCC phase is much lower.

The relation between plastic anisotropy, strain path and phase transformation rate, is now established but still, the observed delay in terms of deformation for α = 45° (see **Fig. 3**) at the beginning of the transformation is not yet explained or whether a coupling with the rate does exist.

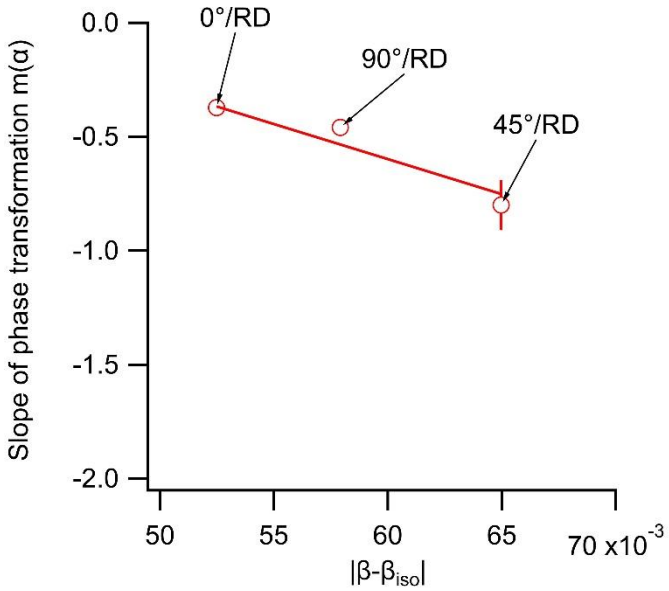

Figure 5: Evolution of the strain-induced FCC to HCP transformation rate in tension with the strain path deviation as compared to the isotropic case ($m(\alpha) = a\times|\beta-\beta_{iso}|+b$ with a = -38 ± 4, b = 1.63 ± 0.26 and R^2 = 0.99).

3.4. *In situ texture evolution, work hardening mechanisms and phase transformation initiation*

In situ crystallographic texture was tracked during tensile tests for each sample (0° /RD (RD), 45° /RD and 90° /RD (TD). **Fig. 6** illustrates $\{00.2\}_{HCP}$ and $\{10.1\}_{HCP}$ PFs for some analysed strain levels. The 0 point represents the unstrained state i.e. as received cobalt sheet, points 1 to 7 match the texture analyses made at different loading steps, and the point 8 corresponds to the final texture after tensile test. **Fig. 6** also shows macroscopic stress-strain curves obtained by the tensile tests for the 3 sampling directions (0° /RD (RD), 45° /RD and 90° /RD (TD°). Evolution of $\{00.2\}_{HCP}$ PF with macroscopic strain shows, whatever α, a homogeneization and a reinforcement of the fiber character of the texture. This basal texture results in an equiaxed central pole, representative of the normal c-axis on the specimen surface. The equiaxiality of the pole is representative of cold-rolled HCP materials with a *c/a* ratio close to 1.633. Consequently, the texture that develops during a tensile deformation reveals the reinforcement of the initial rolling texture. Evolution of $\{10.1\}_{HCP}$ PF with strain shows, whatever *α*, the development of poles in the rolling direction in accordance with the observed evolution of intensities recorded on $\{00.2\}_{HCP}$ PF, supporting the assumption of a reinforcement of this type of texture.

This qualitative analysis highlights a texture evolution which provides an explanation for the phase transformation activation delay for the 45°/RD tensile loading.

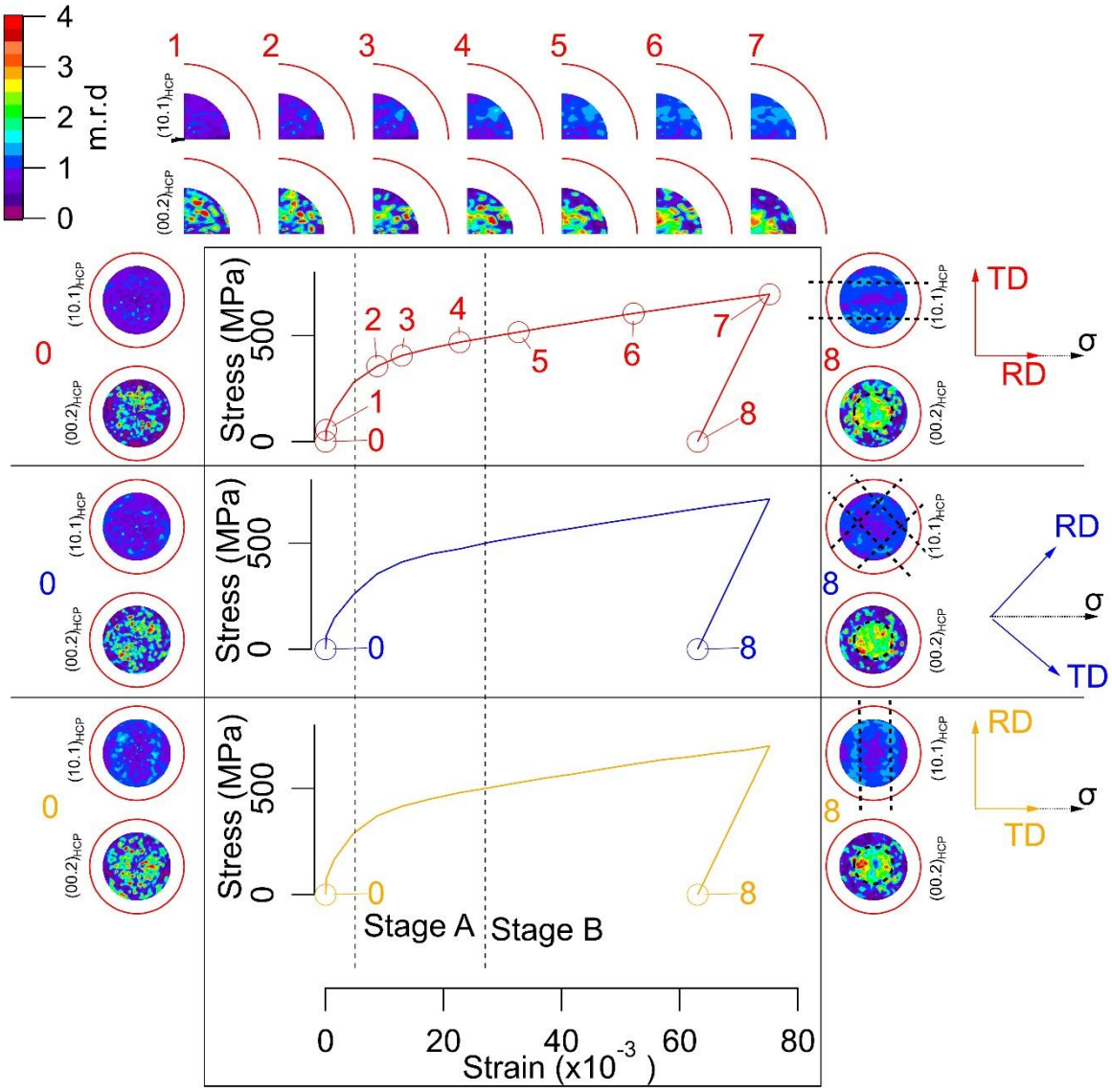

Figure 6: $\{00.2\}_{HCP}$ and $\{10.1\}_{HCP}$ PF evolution during tensile tests. Points 0 and 8 correspond to the initial texture and the residual texture after straining, respectively. Points 1 to 7 correspond to internal texture development during loading. (red color is associated to force applied along the RD (α = 0° /RD), blue for an angle of 45° /RD and green for a mechanical loading parallel to TD (α = 90° /RD)).

As shown in a previous work [58], the combined study of work-hardening mechanisms and phase transformation can be done monitoring the intensity of two diffraction reflections. The $\{00.2\}_{HCP}$ reflection is representative of the main twinning system {10.2}<10.1>, and the $\{10.2\}_{HCP}$ reflection, averaged over a ring corresponding to a declination angle of 5°, is representative of the FCC to HCP phase transformation [7]. For this purpose, the integrated

intensities of the $\{00.2\}_{HCP}$ and $\{10.2\}_{HCP}$ reflections were tracked during the mechanical loading along the three loading directions (**Fig. 7**).

No matter the loading direction, intensity of $\{00.2\}_{HCP}$ reflection starts to increase linearly with the logarithm of the deformation from the beginning of the stage B. This increase reflects the generalization of twinning in this stage and in particular the reorientation due to the $\{10.2\}<10.1>$ system, since it induces an increase of the $\{00.2\}_{HCP}$ population parallel to the surface specimen. The effect of plastic anisotropy on the twinning is clear with a very pronounced increase in the intensity of the $\{00.2\}_{HCP}$ reflection in the case of α = 45° as compared to the other directions which show a similar, but less important, evolution. This may demonstrate an increased twinning activity, favored by the tensile specimen orientation regarding the loading direction.

For 0° /RD and 90°/ RD, intensity of $\{10.2\}_{HCP}$ reflection increases at the end of the elastic domain due to the beginning of the FCC to HCP strain-induced transformation. At the beginning of stage B, intensity reaches a plateau. This trend is similar to the observations of Marx *et al.* [42]. However, these authors did not correlate the work-hardening mechanisms and the intensity evolution. As shown in **Fig. 3**, the overall proportion of FCC continues to decrease during this stage. The $\{10.2\}_{HCP}$ intensity should therefore go on increasing as regard to the phase transformation. Nevertheless, the reorientation due to the activation of the $\{10.2\}<10.1>$ twinning system tends to decrease the $\{10.2\}_{HCP}$ intensity. The stabilization observed is therefore the result of the two competing mechanisms.

For α = 45° /RD, the delayed initiation of the FCC to HCP transformation, identified in **Fig. 3**, is also visible in **Fig. 7** through a significant increase in integrated intensity of $\{10.2\}_{HCP}$ peak at the beginning of stage B. However, in the middle of the stage B, the effect of the twinning mode deformation onto intensity overrides those of the phase transformation, leading to a

sudden drop in intensity. The initial basal texture is not favorable to the {00.1}<1$\bar{2}$.0> slip system activation when the sheet is deformed at 45°/RD.

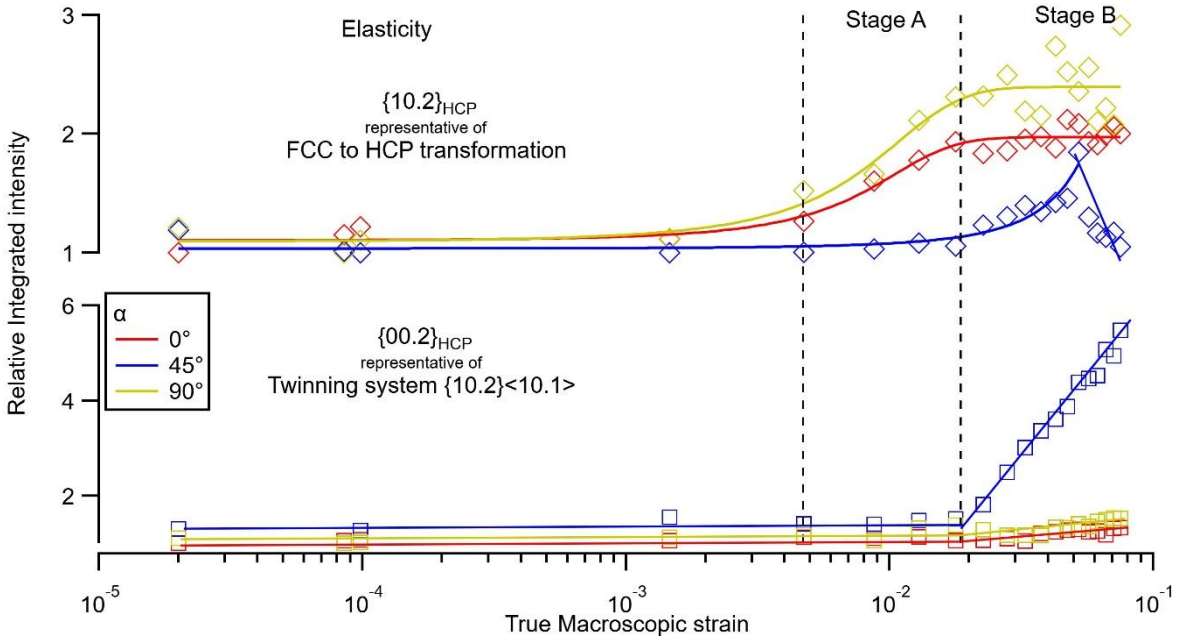

Figure 7: Evolution of the integrated peak intensities of the $\{10.2\}_{HCP}$ reflection (at $\psi = 0°$) and of the $\{00.2\}_{HCP}$ reflection (at $\psi = 5°$) during a tensile test (ψ is the declination angle) for all three directions of specimen collection.

Additional *post mortem* analysis of the work-hardening mechanisms was carried out by EBSD in the case of the tensile specimen at 0°/RD. A quantification of the grain misorientation angles is presented in **Fig. 8** thanks to the orientation analysis of their distribution in the undeformed and deformed states. The as-received cobalt sheet exhibits only two set of populations : the first one displays a misorientation angle corresponding to the Shoji-Nishiyama orientation relationship (71°) between FCC and HCP phases, associated to the martensitic transformation [10], while the second one manifests a 86°misorientation angle, typical of the initial existence of residual tensile twins {10.2}<10.1> due to the cold-rolling process. Above 7.8 % of macroscopic deformation, the twin population increases while the peak located at 71° decreases, highlighting the two mechanisms of twinning and strain-

induced phase transformation (FCC to HCP). A third population appears for misorientation angles lower than 15°. It may be associated with the development of intragranular misorientations due to dislocations and internal stresses [7].

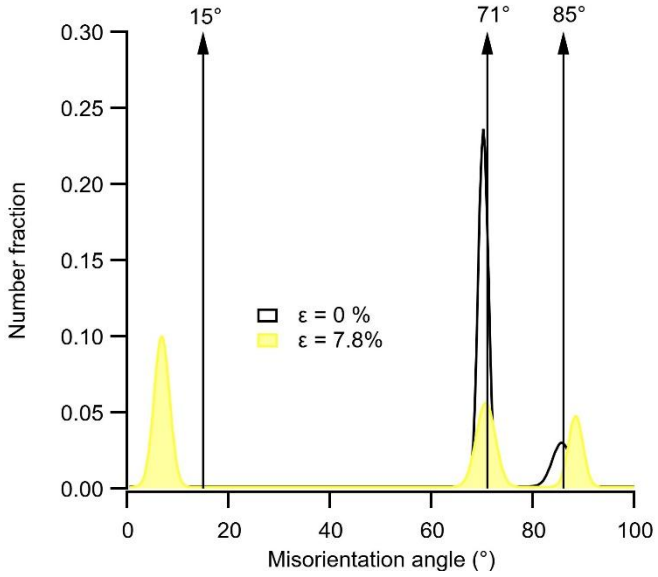

Figure 8: Grain boundary misorientation angle distributions for unstrained state (black solid line) and for a specimen strained in tension at 7.8 % along RD (yellow filled curve).

4. Conclusion

In this work, the strain-induced phase transformation is reported for three sampling directions of a cold-rolled sheet of pure cobalt and for a complex loading which produces higher strain levels than those obtained with tensile tests. The effect of anisotropy is demonstrated to be important for a loading axis at 45° from the RD, with a delayed activation of the FCC to HCP phase transformation and a rate of transformation twice as high as for the rolling and transverse directions. This second observation can be associated with a negative deviation of the strain path as regard to the isotropic case. Moreover, this effect seems to favor twinning deformation mode that ends up transcending phase transformation. For RD (0° /RD) and TD

(90° /RD) directions, whatever the loading mode (tensile or stamping tests), the phase transformation starts at the initiation of plasticity (stage A). In general, the deformation of polycrystalline cobalt is controlled by basal slip and twinning (mainly {10.2}<10.1> tensile twin) but can be accompanied by a plastic strain-induced transformation if the residual FCC phase is not stabilized by a heat treatment. The texture developed during deformation is then a reinforcement of the basal rolling texture.

Acknowledgements

Part of experimental work was performed in the PhD of Nadjib Iskounen (Centrale Nantes 2021) with the support of Marie-José Moya (assistant engineer). The authors would also like to thank Gautier Doumenc and Pascal Paillard (Institut des Matériaux de Nantes Jean Rouxel) for providing access to the EBSD analyses and ENSICAEN for the use of the stamping press.

References

[1] **W. Betteridge**, *The properties of metallic cobalt*, Prog. Mater. Sci. 24, (1980), pp. 51–142. https://doi.org/doi.org/10.1016/0079-6425(79)90004-5.

[2] **L. Rémy, A. Pineau, B. Thomas**, *Temperature dependence of stacking fault energy in close-packed metals and alloys*, Mater. Sci. Eng. 36, (1978), pp. 47–63. https://doi.org/10.1016/0025-5416(78)90194-5.

[3] **A. Seeger**, *Theorie der Kristallplastizität: II. Die Grundstruktur der dichtest gepackten Metalle und ihr Einfluß auf die plastische Verformung*, Z. Für Naturforschung A. 9, (1954), pp. 856–869. https://doi.org/10.1515/zna-1954-1007.

[4] **A. Seeger, H. Kronmüller, O. Boser, M. Rapp**, *Plastische Verformung von Kobalteinkristallen*, Phys. Status Solidi B. 3, (1963), pp. 1107–1125. https://doi.org/10.1002/pssb.19630030617.

[5] **A. Seeger, H. Kronmüller, S. Mader, H. Träuble**, *Work-hardening of hexagonal Close-packed crystals and in the easy glide region of face-centred cubic crystals*, Philos. Mag. J. Theor. Exp. Appl. Phys. 6, (1961), pp. 639–655. https://doi.org/10.1080/14786436108244415.

[6] **M. Martinez, G. Fleurier, F. Chmelík, M. Knapek, B. Viguier, E. Hug**, *TEM analysis of the deformation microstructure of polycrystalline cobalt plastically strained in tension*, Mater. Charact. 134, (2017), pp. 76–83. https://doi.org/10.1016/j.matchar.2017.09.038.

[7] **M. Martinez, E. Hug**, *Characterization of deformation twinning in polycrystalline cobalt: A quantitative analysis*, Materialia. 7, (2019), pp. 100420. https://doi.org/10.1016/j.mtla.2019.100420.
[8] **G. Fleurier, E. Hug, M. Martinez, P.-A. Dubos, C. Keller**, *Size effects and Hall–Petch relation in polycrystalline cobalt*, Philos. Mag. Lett. 95, (2015), pp. 122–130. https://doi.org/10.1080/09500839.2015.1020351.
[9] **M. Martinez Celis, P. Minárik, E. Hug, J. Dorenlor, F. Chmelík, M. Knapek, P. Dobroň**, *Analysis of the twin variant selection in polycrystalline cobalt*, J. Mater. Sci. 56, (2021), pp. 7740–7752. https://doi.org/10.1007/s10853-020-05718-9.
[10] **Y.T. Zhu, X.Y. Zhang, Q. Liu**, *Observation of twins in polycrystalline cobalt containing face-center-cubic and hexagonal-close-packed phases*, Mater. Sci. Eng. A. 528, (2011), pp. 8145–8149. https://doi.org/doi.org/10.1016/j.msea.2011.07.062.
[11] **X.Y. Zhang, Y.T. Zhu, Q. Liu**, *Deformation twinning in polycrystalline Co during room temperature dynamic plastic deformation*, Scr. Mater. 63, (2010), pp. 387–390. https://doi.org/10.1016/j.scriptamat.2010.04.031.
[12] **R. Bauer, E.A. Jaegle, W. Baumann, E.J. Mittemeijer**, *Kinetics of the Allotropic hcp-fcc Phase Transformation in Cobalt*, Philos. Mag. 91, (2010), pp. 437–457. https://doi.org/10.1080/14786435.2010.525541.
[13] **H. Bibring, F. Sebilleau**, *Structure et transformation allotropique du cobalt*, Rev. Métallurgie. 52, (1955), pp. 569–578. https://doi.org/10.1051/metal/195552070569.
[14] **Christian John Wyrill, Hume-Rothery William**, *A theory of the transformation in pure cobalt*, Proc. R. Soc. Lond. Ser. Math. Phys. Sci. 206, (1951), pp. 51–64. https://doi.org/10.1098/rspa.1951.0055.
[15] **H.Th. Hesemann, P. Müllner, E. Arzt**, *Stress and texture development during martensitic transformation in cobalt thin films*, Scr. Mater. 44, (2001), pp. 25–30. https://doi.org/10.1016/S1359-6462(00)00553-4.
[16] **H.Th. Hesemann, P. Müllner, O. Kraft, D. Nowak, S.P. Baker, K. Finkelstein, E. Arzt**, *Texture dependence of the martensitic transformation in cobalt thin films*, Scr. Mater. 48, (2003), pp. 1129–1133. https://doi.org/10.1016/S1359-6462(02)00603-6.
[17] **R. Holt, E. Teghtsoonian**, The influence of the allotropic transformation on the deformation behavior of pure cobalt, in: Metall. Mater. Trans. B, Springer Boston, 1972: pp. 2443–2447. http://dx.doi.org/10.1007/BF02647047 DO - 10.1007/BF02647047 (accessed September 1, 1972).
[18] **C.R. Houska, B.L. Averbach, M. Cohen**, *The cobalt transformation*, Acta Metall. 8, (1960), pp. 81–87. https://doi.org/10.1016/0001-6160(60)90088-2.
[19] **B. Kamel, K. Halim**, *The Effect of Phase Change on the Mechanical Properties of Cobalt Near Its Transformation Temperature*, Phys. Status Solidi B. 15, (1966), pp. 63–69. https://doi.org/10.1002/pssb.19660150104.
[20] **H. Matsumoto**, *Variation in transformation hysteresis in pure cobalt with transformation cycles*, J. Alloys Compd. 223, (1995), pp. L1–L3. https://doi.org/10.1016/0925-8388(95)01523-X.
[21] **H. Matsumoto**, *Effects of transformation-induced defects in cobalt and Ni48Ti52*, Phys. B Condens. Matter. 334, (2003), pp. 112–117. https://doi.org/10.1016/S0921-4526(03)00023-1.
[22] **A. Munier, J.E. Bidaux, R. Schaller, C. Esnouf**, *Evolution of the microstructure of cobalt during diffusionless transformation cycles*, J. Mater. Res. 5, (1990), pp. 769–775. https://doi.org/10.1557/JMR.1990.0769.
[23] **E.A. Owen, D.M. Jones**, *Effetct of the grain size on the crystal structure of cobalt*, Proc. Phys. Soc. B 67, (1954), pp. 456–466.

[24] **J.T. Plewes, K.J. Bachmann**, *The effect of thermomechanical pretreatment on the allotropic transformation in cobalt*, Metall. Trans. 4, (1973), pp. 1729–1734. https://doi.org/10.1007/BF02666203.
[25] **A.E. Ray, S.R. Smith, J.D. Scofielf**, *Study of the phase transformation of cobalt*, J. Phase Equilibria. 12, (1991), pp. 644–648. https://doi.org/doi.org/10.1007/BF02645161.
[26] **F. Sebilleau, H. Bibring, F. Bückle**, *The kinetics and morphology of the allotropic transformation of cobalt*, J. Inst. Met. 87, (1958), pp. 71.
[27] **F. Sebilleau, H. Bibring**, *Structure and allotropic transformation of cobalt*, Rev. Métallurgie. 52, (1955), pp. 569.
[28] **F. Sebilleau, H.Bibring**, *The allotropic transformation of cobalt*, Inst. Met. Monogr. 18, (1956), pp. 209–217.
[29] **J. Sort, S. Suriñach, J.S. Muñoz, M.D. Baró, M. Wojcik, E. Jedryka, S. Nadolski, N. Sheludko, J. Nogués**, *Role of stacking faults in the structural and magnetic properties of ball-milled cobalt*, Phys. Rev. B. 68, (2003), pp. 014421.
[30] **X. Wu, N. Tao, Y. Hong, J. Lu, K. Lu**, *[gamma]-->[epsilon] martensite transformation and twinning deformation in fcc cobalt during surface mechanical attrition treatment*, Scr. Mater. 52, (2005), pp. 547–551.
[31] **J.-C. Zhao, M.R. Notis**, *Kinetics of the fcc to hcp phase transformation and the formation of martensite in pure cobalt*, Scr. Metall. Mater. 32, (1995), pp. 1671–1676. https://doi.org/10.1016/0956-716X(95)00253-R.
[32] **C.C. Sanderson**, *Deformation of polycristalline cobalt*, PhD Thesis, University of British Columbia, (1972).
[33] **G. Bouquet, B. Dubois**, *Influence of the F.C.C. phase retained at room temperature on the mechanical properties of cobalt*, Scr. Metall. 12, (1978), pp. 1079–1081. https://doi.org/10.1016/0036-9748(78)90078-9.
[34] **L. Habraken**, *Propriétés du cobalt et de ses alliages*, Tech. Ing. 505–506, (1979), pp. 1–19 et 1–16.
[35] **R. Holt, E. Teghtsoonian**, The tensile deformation of cobalt single crystals in the fcc phase, in: Metall. Mater. Trans. B, Springer Boston, 1972: pp. 1621–1626. http://dx.doi.org/10.1007/BF02643054 DO - 10.1007/BF02643054 (accessed June 1, 1972).
[36] **A.A. Karimpoor**, *Mechanical properties of bulk nanocrystalline hexagonal cobalt electrodeposits*, University of TorontoEditor, (2001).
[37] **L.D. Sokolov, A.N. Gladkikh, V.A. Skudnov, V.M. Solenov**, *Mechanical properties of cobalt at different temperatures and deformation rates*, Met. Sci. Heat Treat. 11, (1969), pp. 626–628.
[38] **A.G. Zhou, D. Brown, S. Vogel, O. Yeheskel, M.W. Barsoum**, *On the kinking nonlinear elastic deformation of cobalt*, Mater. Sci. Eng. A. 527, (2010), pp. 4664–4673. https://doi.org/doi.org/10.1016/j.msea.2010.04.048.
[39] **E. Hug, C. Keller**, *Size effects and magnetoelastic couplings: a link between Hall–Petch behaviour and coercive field in soft ferromagnetic metals*, Philos. Mag. 99, (2019), pp. 1297–1326. https://doi.org/10.1080/14786435.2019.1580397.
[40] **E. Hug, C. Keller, P.-A. Dubos, M.M. Celis**, *Size effects in cobalt plastically strained in tension: impact on gliding and twinning work hardening mechanisms*, J. Mater. Res. Technol. (2021), pp. S2238785421001058. https://doi.org/10.1016/j.jmrt.2021.01.105.
[41] **A. Zhou**, *Kinking Nonlinear Elastic Solids : Theory and Experiments*, Drexel UniversityEditor, (2008).
[42] **V.M. Marx, C. Kirchlechner, B. Breitbach, M.J. Cordill, D.M. Többens, T. Waitz, G. Dehm**, *Strain-induced phase transformation of a thin Co film on flexible substrates*, Acta Mater. 121, (2016), pp. 227–233. https://doi.org/10.1016/j.actamat.2016.09.015.

[43] **P.-A. Dubos, J. Fajoui, N. Iskounen, M. Coret, S. Kabra, J. Kelleher, B. Girault, D. Gloaguen**, *Temperature effect on strain-induced phase transformation of cobalt*, Mater. Lett. 281, (2020), pp. 128812. https://doi.org/10.1016/j.matlet.2020.128812.
[44] **L. Rémy, A. Pineau**, *Twinning and strain-induced f.c.c. → h.c.p. transformation on the mechanical properties of Co-Ni-Cr-Mo alloys*, Mater. Sci. Eng. 26, (1976), pp. 123–132. https://doi.org/10.1016/0025-5416(76)90234-2.
[45] **B.B. Straumal, A.A. Mazilkin, B. Baretzky, G. Schütz, E. Rabkin, R.Z. Valiev**, *Accelerated Diffusion and Phase Transformations in Co–Cu Alloys Driven by the Severe Plastic Deformation*, Mater. Trans. 53, (2012), pp. 63–71. https://doi.org/10.2320/matertrans.MD201111.
[46] **P.-A. Dubos, E. Hug, S. Thibault, M. Ben Bettaieb, C. Keller**, *Size Effects in Thin Face-Centered Cubic Metals for Different Complex Forming Loadings*, Metall. Mater. Trans. A. 44, (2013), pp. 5478–5487. https://doi.org/10.1007/s11661-013-1892-7.
[47] **P.A. Dubos, G. Fleurier, E. Hug**, *An Experimental Investigation of the Size Effects in Forming Processes of High-Purity Thin Metallic Sheets*, Mater. Sci. Forum. 879, (2017), pp. 459–464. https://doi.org/10.4028/www.scientific.net/MSF.879.459.
[48] **P. Vedoya, A. Pochettino, R. Penelle**, *Plastic Anisotropy of Titanium, Zirconium and Zircaloy 4 Thin Sheets*, Textures Microstruct. 8, (1988), pp. 601–610. https://doi.org/10.1155/TSM.8-9.601.
[49] **F. Kocks, C. Tomé, H.-R. Wenk**, Texture and Anisotropy. Preferred Orientations in Polycrystals and Their Effect on Material Properties, 2000.
[50] **W.A. Rachinger**, *A Correction for the 1 2Doublet in the Measurement of Widths of X-ray Diffraction Lines*, J. Sci. Instrum. 25, (1948), pp. 254–255. https://doi.org/10.1088/0950-7671/25/7/125.
[51] **M.J. Buerger**, *The Correction of X-Ray Diffraction Intensities for Lorentz and Polarization Factors*, Proc. Natl. Acad. Sci. 26, (1940), pp. 637–642. https://doi.org/10.1073/pnas.26.11.637.
[52] **H.-R. Wenk, S. Matthies, J. Donovan, D. Chateigner**, *BEARTEX: a Windows-based program system for quantitative texture analysis*, J. Appl. Crystallogr. 31, (1998), pp. 262–269. https://doi.org/10.1107/S002188989700811X.
[53] **S.L. Shang, W.Y. Wang, Y. Wang, Y. Du, J.X. Zhang, A.D. Patel, Z.K. Liu**, *Temperature-dependent ideal strength and stacking fault energy of fcc Ni: a first-principles study of shear deformation*, J. Phys. Condens. Matter. 24, (2012), pp. 155402. https://doi.org/10.1088/0953-8984/24/15/155402.
[54] **J.T. Bonarski, M. Wróbel, K. Pawlik**, *Quantitative phase analysis of duplex stainless steel using incomplete pole figures*, Mater. Sci. Technol. 16, (2000), pp. 657–662. https://doi.org/10.1179/026708300101508234.
[55] **C. H. MacGillavry, G D. Rieck**, International Tables for X-Ray Crystallography vol 3, n.d. http://archive.org/details/InternationalTablesForX-rayCrystallographyVol3.
[56] **A. Col**, *Emboutissage des tôles. Importance des modes de déformations*, Tech. Ing. 180, (2002), pp. 1–20.
[57] **Z. Marciniak, J.L. Duncan, S.J. Hu**, 1 - Material properties, in: Mech. Sheet Met. Form. Second Ed., Butterworth-Heinemann, Oxford, 2002: pp. 1–13.
[58] **N. Iskounen, P.A. Dubos, J. Fajoui, M. Coret, M.-J. Moya, B. Girault, N. Barrier, N. Bruzy, E. Hug, D. Gloaguen**, *Experimental investigation of allotropic transformation of cobalt: influence of temperature cycle, mechanical loading and starting microstructure*, Metall. Mater. Trans. A. (2021),.

609

Figures captions:

Figure 1: Microstructural analysis of the as-received material**:** (a) EBSD map of phase distribution and band contrast. Distribution of grain size for each phase. HCP phase is colored in red and FCC phase in green. (b) XRD crystallographic textures of the HCP phase determined from the orientation distribution functions calculated by the WIMW method implanted in the BEARTEX software.

Figure 2: Description of the Nakazima test: (a) height of the part after stamping and location of the analysis points by XRD (cross and circle marker for measurements in RD and TD, respectively), (b) decomposition of the principal components of the macroscopic strain fields (ε_I: in-plane major strain (along RD), ε_{II}: in-plane minor strain (along TD), $\varepsilon_{III}=-\varepsilon_I-\varepsilon_{II}$: in the thickness strain and corresponding ε_{eq} von Mises equivalent strain), (c) evolution of the strain path β versus the location on the section.

Figure 3: FCC phase proportion (normalized to the initial retained FCC phase) and work-hardening rate evolutions under tensile testing for different angles between the load axis and the rolling direction (RD): 0° /RD (RD), 45° /RD and 90° /RD (TD°).

Figure 4: Influence of different biaxial loading scenarios on the phase transformation. Evolution of the FCC phase ratio along the rolling and transverse directions (filled squares) of a stamped sample, superposed on the in situ tensile test results (circles).

Figure 5: Evolution of the strain-induced FCC to HCP transformation rate in tension with the strain path deviation as compared to the isotropic case ($m(\alpha) = a\times|\beta-\beta_{iso}|+b$ with $a = -38 \pm 4$, $b = 1.63 \pm 0.26$ and $R^2 = 0.99$).

Figure 6: $\{00.2\}_{HCP}$ and $\{10.1\}_{HCP}$ PF evolution during tensile tests. Points 0 and 8 correspond to the initial texture and the residual texture after straining, respectively. Points 1 to 7 correspond to internal texture development during loading. (red color is associated to force applied along the RD ($\alpha = 0°$ /RD), blue for an angle of 45° /RD and green for a mechanical loading parallel to TD ($\alpha = 90°$ /RD)).

Figure 7: Evolution of the integrated peak intensities of the $\{10.2\}_{HCP}$ reflection (at $\psi = 0°$) and of the $\{00.2\}_{HCP}$ reflection (at $\psi = 5°$) during a tensile test (ψ is the declination angle) for all three directions of specimen collection.

Figure 8: Grain boundary misorientation angle distributions for unstrained state (black solid line) and for a specimen strained in tension at 7.8 % along RD (yellow filled curve).

Tables captions:

Table 1: Review of the main coefficients characterizing elastic and plastic anisotropies determined for polycrystalline specimens (E: Young modulus, ν: Poisson coefficient, α: direction of specimen collection, r: Lankford coefficient, β; strain path, $|\beta-\beta_{iso}|$: strain path deviation, r_{mean}: mean plastic anisotropy coefficient, Δr: planar plastic anisotropy coefficient).

Table 2: Coefficients of equation (8) with standard deviations (u) and linear regression coefficient (R^2) as a function of the loading axis misorientation regarding the RD.